AIAA JOURNAL
Vol. 33, No. 2, February 1995

Comparison of Higher Resolution Euler Schemes for Aeroacoustic Computations

San-Yih Lin* and Yan-Shin Chin†
National Cheng Kung University, Tainan 70101, Taiwan, Republic of China

Modified finite volume methods of Osher and Chakravarthy (MOC) and Sanders and Li (MSL) and a finite element method of Lin and Chin are investigated on several aeroacoustic problems. Higher order accuracy is obtained with the monotonic upwind-centered scheme for conservation laws approach. The tested problems include oblique shock reflection, linear wave convection, monopole radiation, vortex preservation, and blade-vortex interaction. Based on the order of accuracy, stability, grid nonuniformity, and dissipation property of each scheme, it is concluded that the MOC scheme is the most suitable scheme among the schemes tested for aeroacoustic computations. We also conclude that the MSL scheme needs to be improved on problems of convergence and small wiggles before it is used in computational aeroacoustics. In the blade-vortex interaction problem, two sound waves, transonic and compressibility waves, found in recent experiments are simulated.

I. Introduction

In recent years, considerable progress has been made in the numerical analysis of fluid dynamics. Usually, numerical methods which solve the Euler/Navier–Stokes equations for aerodynamic flows fall into three major classes: finite difference, finite volume, and finite element methods. Recently, successful methods have employed higher order upwind interpolations and limiter functions to obtain algorithms possessing higher resolution and higher stability bounds. The inherently dissipative nature of upwind schemes and limiter functions is beneficial at or near shock waves. Specifically, the implementation of limiter functions make schemes more stable for computing solutions with strong shock waves. In general, an upwind scheme with a limiter function is formally second- or third-order accurate but is locally first-order accurate in regions of high localized gradients (such as shocks) and in many cases at local extrema also. The loss of formal accuracy near shocks is not usually serious, but for aeroacoustic calculations the dissipation at extrema will be harmful.

Upwind schemes may be classified into two classes: monotonic upwind-centered scheme for conservation laws (MUSCL) and nonMUSCL.[1–4] The present work is focused on the MUSCL-based schemes. We have studied the performance of the following three basic schemes: 1) the finite element method of Lin and Chin (LC)[5] and Lin et al.,[6] 2) the finite volume method of Osher and Chakravarthy (OC)[7], and 3) the finite volume method of Sanders and Li (SL).[8,9] The popularity of the OC scheme for aeroacoustic computations is likely to increase since it is formally of third order and is stable in the computation of strong shock waves. The SL scheme is formally of fourth order and is a suitable method for the aeroacoustic computation of low-speed flows. An overall assessment of this scheme is available in Refs. 8 and 9. The LC scheme is formally of second order for both uniform and nonuniform meshes. This scheme has been extensively tested on both inviscid and viscous flows.[5,6] It has been shown that the scheme is capable of computation of steady and unsteady flows. In this paper, we have modified the limiter functions in the OC and SL schemes to obtain two new schemes, the modified OC (MOC) and the modified SL (MSL) schemes.

In this effort a detailed investigation is performed to evaluate the capability of those schemes. Several test problems are studied, including oblique shock reflection, linear wave convection, monopole radiation, vortex preservation, and blade-vortex interaction. Details of each scheme are presented in Sec. II. Numerical results and comparisons of those schemes are presented in Sec. III. For the blade vortex interaction problem, two sound waves, transonic and compressibility waves described by Lent et al.,[10] are simulated.

Received Dec. 23, 1993; revision received April 11, 1994; accepted for publication April 22, 1994.

*Professor, Institute of Aeronautics and Astronautics. Member AIAA.
†Post Doctor, Institute of Aeronautics and Astronautics.

II. Theoretical Model

A. Governing Equation

Flows of a two-dimensional, compressible, inviscid fluid can be described in conservation form by the Euler equations

$$W_t + F_x + G_y = 0 \tag{1}$$

where

$$W = \begin{pmatrix} \rho \\ \rho u \\ \rho v \\ \rho e \end{pmatrix}, \qquad F = \begin{pmatrix} \rho u \\ \rho u^2 + p \\ \rho uv \\ u(\rho e + p) \end{pmatrix}$$

$$G = \begin{pmatrix} \rho v \\ \rho uv \\ \rho v^2 + p \\ v(\rho e + p) \end{pmatrix}$$

Here p, ρ, u, v, and e are the pressure, density, x- and y-directional velocity components, and the total energy per unit mass, respectively. The pressure p is given by the equation of state for a perfect gas

$$p = (\gamma - 1)\left[\rho e - \tfrac{1}{2}\rho(u^2 + v^2)\right] \tag{2}$$

where γ (= 1.4 for air) is the ratio of specific heats.

B. Numerical Schemes

The numerical schemes discussed are of the MUSCL type. The spatial accuracy of each scheme depends on the evaluation of flow fluxes at the grid interface. In this paper, the implementation of each scheme is demonstrated by a one-dimensional Cartesian flux F at a surface $i-\frac{1}{2}$, where i is the index of grid in x direction. The extension to multidimensional general coordinates is straightforward. First, the state of the flow at each interface is described by two vectors of conserved variables on either side, $\boldsymbol{W}^L$ and $\boldsymbol{W}^R$. These values are obtained by finite element formulations for the LC scheme, by upwind extrapolation for the OC scheme, or by center interpolation for the SL scheme. The flux at the interface is then obtained by Roe's approximate Riemann solver[11]:

$$F_{i-\frac{1}{2}} = \tfrac{1}{2}[F(\boldsymbol{W}^L) + F(\boldsymbol{W}^R) - R|\Lambda|L(\boldsymbol{W}^R - \boldsymbol{W}^L)] \tag{3}$$

where L and R are the left and right eigenmatrices of the Jacobian matrix A at the Roe averaged values of $\boldsymbol{W}^R$ and $\boldsymbol{W}^L$, and Λ is the corresponding diagonal matrix of eigenvalues. As Harten[2] pointed out, one needs to employ the entropy correction for Roe's solver when the eigenvalues at the Roe-averaged state vanish. After the space discretizations are performed by each scheme, Eq. (1) becomes an ordinary differential system. A second-order Runge-Kutta scheme[12] is used for the time integration. The characteristic boundary condition is used on the far-field boundary. The solid surface boundary conditions involve no penetration for velocity, extrapolation for density, and solution of the momentum equation for pressure.

Lin and Chin Finite Element Scheme

The formula for this scheme may be written as

$$\boldsymbol{W}^R_{i-\frac{1}{2}} = W_i - \tilde{W}_i^{(\mathrm{mod})}, \qquad \boldsymbol{W}^L_{i+\frac{1}{2}} = W_i + \tilde{W}_i^{(\mathrm{mod})} \tag{4}$$

where $\tilde{W}^{(\mathrm{mod})}$ introduces the minmod limiter

$$\tilde{W}_i^{(\mathrm{mod})} = \mathrm{minmod}\left(\tilde{W}_i, \Delta_{i+\frac{1}{2}} W, \Delta_{i-\frac{1}{2}} W\right) \tag{5}$$

where $\Delta_{i+\frac{1}{2}} W = W_{i+1} - W_i$ and the minmod function is defined as

$$\mathrm{minmod}(x, y, z) = \mathrm{sgn}(x) \cdot \max\{0, \min[|x|, y \cdot \mathrm{sgn}(x), z \cdot \mathrm{sgn}(x)]\} \tag{6}$$

where W_i and $\tilde{W}_i$ represent the mean value and normalized i coordinate derivative respectively. Since $\tilde{W}_i$ was obtained by an integral formulation, we refer to the LC scheme as a finite element scheme. The details were presented in Refs. 5 and 6. This scheme can capture shocks well, although it is only second-order accurate in space.

Osher and Chakravarthy Finite Volume Scheme

The formula for this scheme may be written as

$$\boldsymbol{W}^R_{i-\frac{1}{2}} = W_i - a_i \cdot \left[(c_i - 2 \cdot \kappa \cdot b_i) \cdot \Delta_{i+\frac{1}{2}} W + \frac{1}{c_i} \cdot (1 + 2 \cdot \kappa \cdot b_i) \cdot \Delta_{i-\frac{1}{2}} W\right]$$

$$\boldsymbol{W}^L_{i+\frac{1}{2}} = W_i + a_i \cdot \left[(c_i + 2 \cdot \kappa \cdot b_i) \cdot \Delta_{i+\frac{1}{2}} W + \frac{1}{c_i} \cdot (1 - 2 \cdot \kappa \cdot b_i) \cdot \Delta_{i-\frac{1}{2}} W\right] \tag{7}$$

where κ is a constant, $-1 \le \kappa \le 1$, and the nonuniformity of cell sizes is taken into account in a_i, b_i, and c_i (Ref. 13). If ℓ_i represents the width of the ith cell, then

$$a_i = \frac{\ell_i}{\ell_{i+1} + 2 \cdot \ell_i + \ell_{i-1}}$$

$$b_i = \frac{\ell_i}{\ell_i + \ell_{i+1}}$$

$$c_i = \frac{\ell_i + \ell_{i-1}}{\ell_i + \ell_{i+1}} \tag{8}$$

For a linear conservation law problem with a uniform mesh, the OC scheme becomes the standard Osher and Chakravarthy scheme.[7] In this paper, a value $\kappa = \frac{1}{3}$ is used so that the scheme is formally third order. To enforce the stability of the OC scheme, the following slope limiter is used to replace $\Delta_{i+\frac{1}{2}} W$ and $\Delta_{i-\frac{1}{2}} W$ in Eq. (7)

$$\tilde{\Delta}_{i+\frac{1}{2}} W = \mathrm{minmod}\left[\Delta_{i+\frac{1}{2}} W, c_i^{-1} \Delta_{i-\frac{1}{2}} W\right]$$

$$\tilde{\tilde{\Delta}}_{i-\frac{1}{2}} W = \mathrm{minmod}\left[\Delta_{i-\frac{1}{2}} W, c_i \Delta_{i+\frac{1}{2}} W\right] \tag{9}$$

Modified Osher and Chakravarthy Finite Volume Scheme

In this scheme, $\boldsymbol{W}^R$ and $\boldsymbol{W}^L$ obtained in Eq. (7) use the following limiter on $\boldsymbol{W}^R$ and $\boldsymbol{W}^L$ for stability:

$$\boldsymbol{W}^{R,(\mathrm{mod})}_{i-\frac{1}{2}} = W_i - \mathrm{minmod}\left(W_i - \boldsymbol{W}^R_{i-\frac{1}{2}}, \Delta_{i+\frac{1}{2}} W, \Delta_{i-\frac{1}{2}} W\right)$$

$$\boldsymbol{W}^{L,(\mathrm{mod})}_{i+\frac{1}{2}} = W_i + \mathrm{minmod}\left(\boldsymbol{W}^L_{i+\frac{1}{2}} - W_i, \Delta_{i+\frac{1}{2}} W, \Delta_{i-\frac{1}{2}} W\right) \tag{10}$$

Theoretically, the MOC scheme is very similar to the OC scheme. However, the MOC scheme is simpler and generates better numerical results than does the OC scheme.

Modified Sanders and Li Finite Volume Scheme

First, $\boldsymbol{W}^R$ and $\boldsymbol{W}^L$ are obtained as in Eq. (7), and the definition

$$W_{i-\frac{1}{2}} = \tfrac{1}{2}\left(\boldsymbol{W}^R_{i-\frac{1}{2}} + \boldsymbol{W}^L_{i-\frac{1}{2}}\right) \tag{11}$$

is made. In a manner similar to the MOC scheme, the MSL scheme applies the following limiter on $\boldsymbol{W}^R$ and $\boldsymbol{W}^L$ for stability:

$$\boldsymbol{W}^{R,(\mathrm{mod})}_{i-\frac{1}{2}} = W_i - \mathrm{minmod}\left(W_i - W_{i-\frac{1}{2}}, \Delta_{i+\frac{1}{2}} W, \Delta_{i-\frac{1}{2}} W\right)$$

$$\boldsymbol{W}^{L,(\mathrm{mod})}_{i+\frac{1}{2}} = W_i + \mathrm{minmod}\left(W_{i+\frac{1}{2}} - W_i, \Delta_{i+\frac{1}{2}} W, \Delta_{i-\frac{1}{2}} W\right) \tag{12}$$

The MSL scheme is a central scheme and is formally of fourth-order. The original scheme proposed by Sander and Li uses more complicated limiter processes.[8,9] The minmod limiters in Eqs. (5), (10), and (12) belong to the Osher-type limiter.[3]

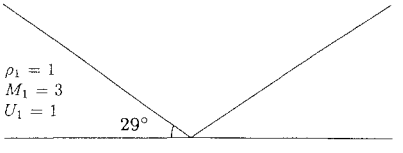

Fig. 1 Problem statement for the oblique shock reflection.

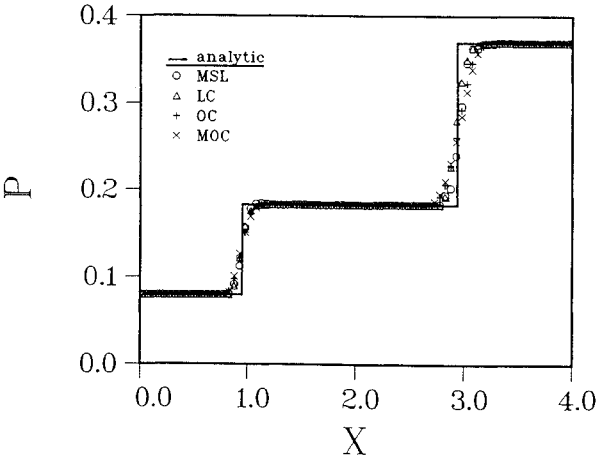

Fig. 2 Pressure distribution along the wall for the oblique shock reflection.

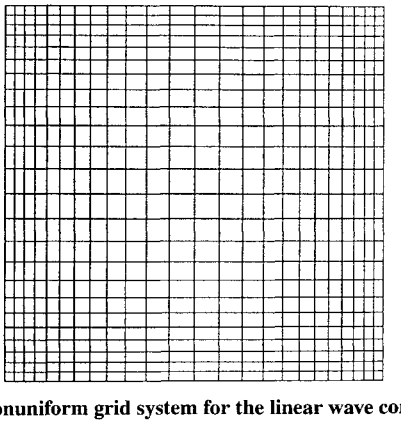

Fig. 3 Nonuniform grid system for the linear wave convection.

III. Numerical Results

A. Oblique Shock Reflection

An oblique shock wave impinges on a solid surface with an incident shock wave angle of 29 deg and inflow Mach number of 3 (Ref. 14). The exact solution has three subregions with a uniform state as shown in Fig. 1. The computational domain is $(0, 4) \times (0, 1)$. A uniform grid of 80×20 is used in this computation. Calculations with each of the schemes are compared with the exact solution for pressure at a fixed y station, $y = 0.475$. Figure 2 shows the results of four schemes. The performance of the LC scheme is slightly better than that of the MSL scheme. Also, the L^2-norm convergence history of the MSL scheme can only reach up to 10^{-2}. Although unsteady flows are of primary interest in this paper, a converged solution is usually needed before an unsteady flow calculation is started in order to avoid generating small disturbances in aeroacoustic calculations. Therefore we conclude that convergence of the MSL scheme is a problem which needs further study. The performance of the MOC and OC schemes are very similar. Figure 2 indicates that the capability of shock capturing by the LC and MSL schemes is better than that of the OC and MOC schemes in this strong shock case.

B. Two-Dimensional Linear Wave Convection

A linear wave convection problem is used here to investigate in detail the effects of limiter function and grid stretching of each scheme. The equation governing linear wave convection is given by

$$u_t + u_x + u_y = 0, \quad \text{in } (0, T) \times \Omega \tag{13}$$

where the domain Ω is a square of $(-1,1) \times (-1,1)$. The computational domain is selected such that the periodic boundary condition can be applied easily. Two initial conditions are tested in this case. The first condition is purely sinusoidal

$$u(t = 0, x, y) = \bar{u} + u' \sin[2\pi(x + y)] \tag{14}$$

where $\bar{u}$ and u' are chosen as 1 and 0.005, respectively. In this case, both uniform and nonuniform grids are used. Figure 3 shows the nonuniform grid with 25×25 grid points. Since the time accuracy is only second order, the time step is taken to be small. Comparison of results is done at $t = 8$. Figure 4 shows contour plots computed with the MOC scheme. It can be seen that good accuracy is achieved on the uniform grid but that a small disturbance has appeared on the nonuniform grid. A larger disturbance is observed in Fig. 4d in which the grid nonuniformity is not considered, i.e., when $a_i = \frac{1}{4}$,

Table 1 Order of accuracy of the MSL scheme without limiter

N	Uniform L_2 error	Order	Nonuniform L_2 error	Order
16	5.2×10^{-4}		7.9×10^{-4}	
24	9.4×10^{-5}	3.9	2.6×10^{-4}	2.8
32	3.0×10^{-5}	4.0	1.4×10^{-4}	2.2

Table 2 Order of accuracy of the MSL scheme

N	Uniform L_2 error	Order	Nonuniform L_2 error	Order
16	1.2×10^{-3}		1.5×10^{-3}	
24	4.0×10^{-4}	2.7	6.4×10^{-4}	2.1
32	3.0×10^{-4}	1.0	4.3×10^{-4}	1.4

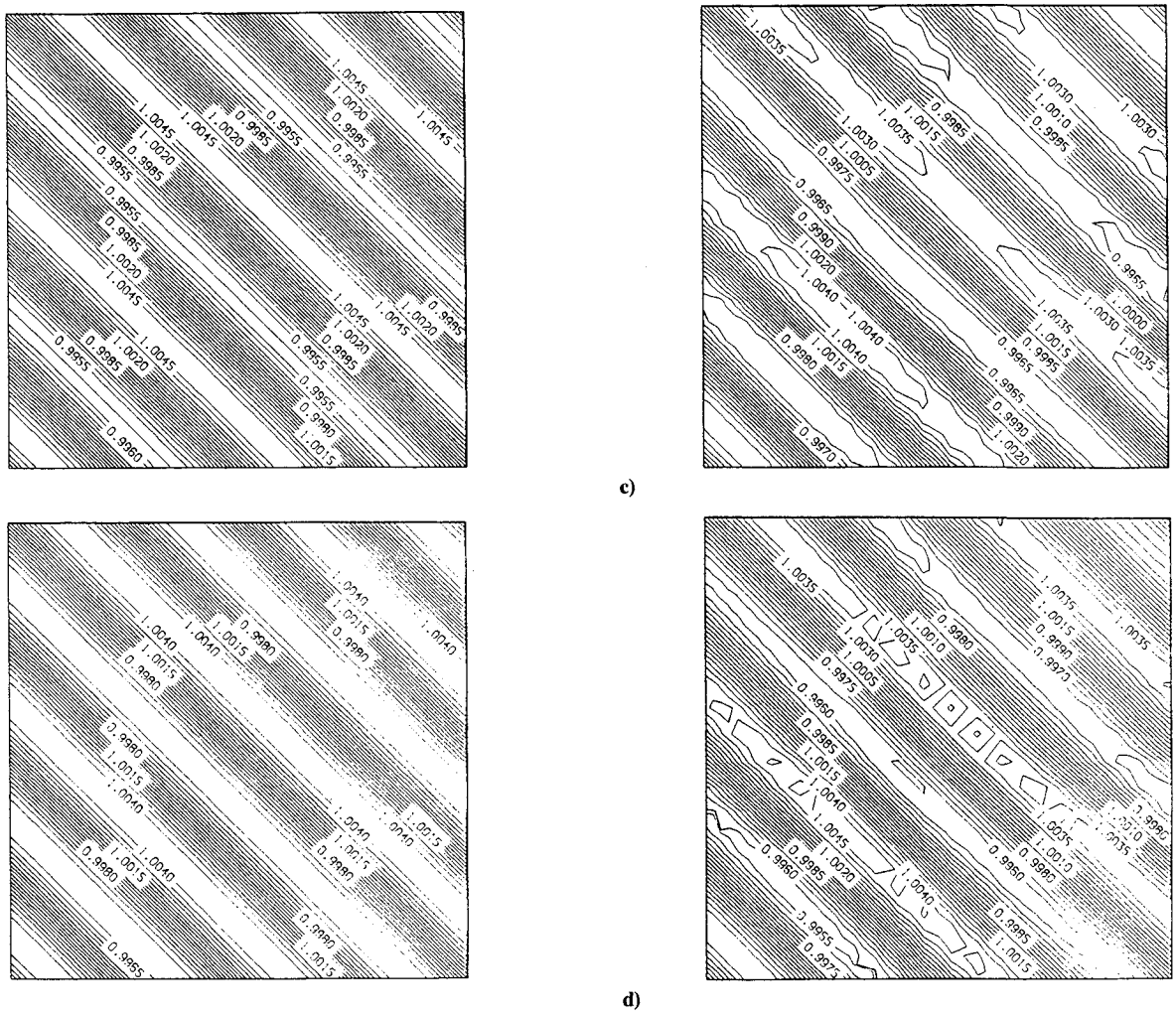

Fig. 4 Contour plots computed with the MOC scheme: a) exact solution, b) uniform-grid solution, c) nonuniform-grid solution with considering grid nonuniformity, and d) nonuniform-grid solution without considering grid nonuniformity.

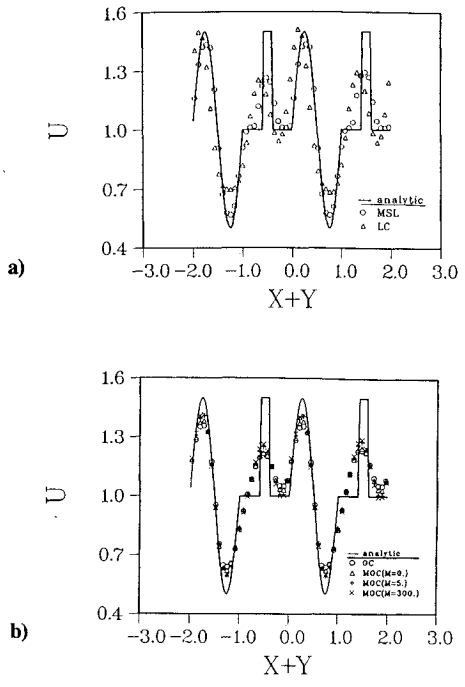

Fig. 5 Contour plots for the linear wave convection with the second initial data obtained by schemes: a) MSL and LC and b) OC and MOC.

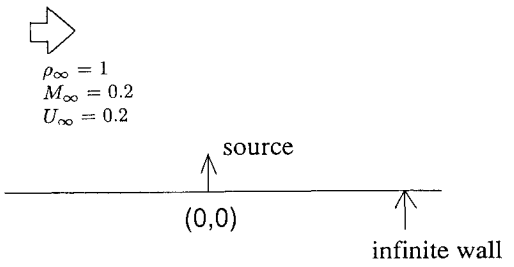

Fig. 6 Schematic of the monopole radiation in a compressible stream.

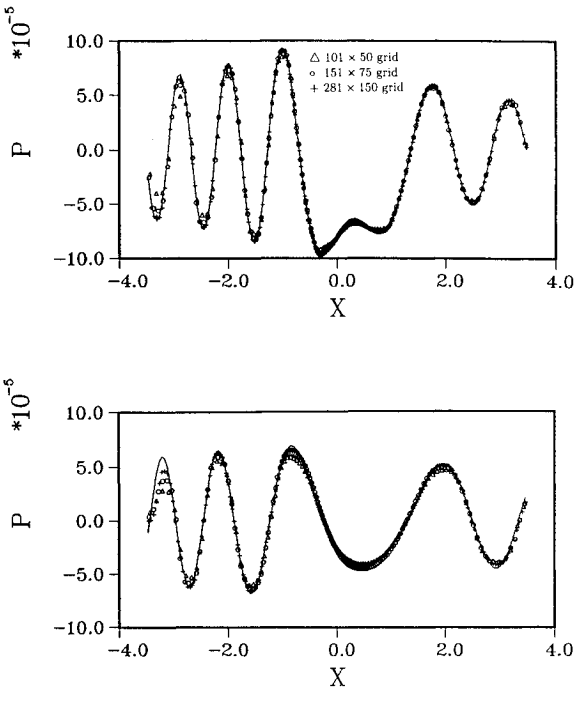

Fig. 7 Pressure plots at two y levels obtained by the MSL scheme: a) $y = 1.26$ and b) $y = 2.508$.

Table 3 Order of accuracy of the MSL scheme without nonuniformity effect

N	No limit L_2 error	Order	Limiter L_2 error	Order
16	9.8×10^{-4}		2.3×10^{-3}	
24	4.8×10^{-4}	2.3	1.3×10^{-3}	1.5
32	2.2×10^{-4}	1.9	8.4×10^{-4}	1.4

Table 4 Order of accuracy of the OC scheme without limiter

N	Uniform L_2 error	Order	Nonuniform L_2 error	Order
16	1.4×10^{-3}		1.6×10^{-3}	
24	4.9×10^{-4}	2.5	7.5×10^{-4}	1.8
32	2.1×10^{-4}	2.8	4.6×10^{-4}	1.7

Table 5 Order of accuracy of the OC scheme

N	Uniform L_2 error	Order	Nonuniform L_2 error	Order
16	2.1×10^{-3}		2.3×10^{-3}	
24	8.4×10^{-4}	2.3	1.2×10^{-3}	1.5
32	4.0×10^{-4}	2.5	8.0×10^{-4}	1.5

Table 6 Order of accuracy of the MOC scheme

N	Uniform L_2 error	Order	Nonuniform L_2 error	Order
16	1.9×10^{-3}		2.1×10^{-3}	
24	6.8×10^{-4}	2.5	1.0×10^{-3}	1.7
32	3.1×10^{-4}	2.7	6.6×10^{-4}	1.6

Table 7 Order of accuracy of the LC scheme without limiter

N	Uniform L_2 error	Order	Nonuniform L_2 error	Order
16	1.7×10^{-3}		1.9×10^{-3}	
24	9.0×10^{-4}	1.6	1.1×10^{-3}	1.3
32	5.3×10^{-4}	1.8	8.0×10^{-4}	1.2

Table 8 Order of accuracy of of the LC scheme

N	Uniform L_2 error	Order	Nonuniform L_2 error	Order
16	2.1×10^{-3}		2.3×10^{-3}	
24	1.0×10^{-3}	1.7	1.3×10^{-3}	1.3
32	6.3×10^{-4}	1.7	9.6×10^{-4}	1.7

$b_i = \frac{1}{2}$, and $c_i = 1$ in Eq. (8). The performance of the MSL, OC, and LC schemes is very similar to that of the MOC scheme. Table 1 shows the errors and orders of accuracy using the MSL scheme without a limiter on the uniform and nonuniform grids. The errors are obtained by comparing with exact solutions. One can see that the grid nonuniformity results are about 1.5 times less than the order of accuracy obtained using the uniform grid. Table 2 shows the errors and orders of accuracy using the MSL scheme with the limiter on the uniform and nonuniform grids. By comparing Tables 1 and 2, the effect of the limiter function can be clearly demonstrated. At this point, one may use a total variation bounded (TVB) scheme instead using a total variation diminishing (TVD) scheme to reduce the effect of the limiter function, which we will study later. Table 3 shows the errors and orders of accuracy using the MSL scheme without considering grid nonuniformity effects, i.e., by setting $a_i = \frac{1}{4}$, $b_i = \frac{1}{2}$, and $c_i = 1$ in Eq. (8). It indicates the importance of a scheme accounting for the nonuniformity effect. Tables 4 and 5 show the errors and orders of accuracy of the OC scheme without and with the limiter. Table 6 shows the errors and orders of accuracy of the MOC scheme. The performance of the MOC scheme is slightly better than that of the OC scheme. Tables 7 and 8

Table 9 Three grid systems of monopole radiation

$N \times M$	$\Delta x_{\min}$	$\Delta y_{\min}$
101×50	3.6×10^{-2}	3.6×10^{-2}
151×75	2.0×10^{-2}	2.0×10^{-2}
281×150	8.9×10^{-3}	7.7×10^{-3}

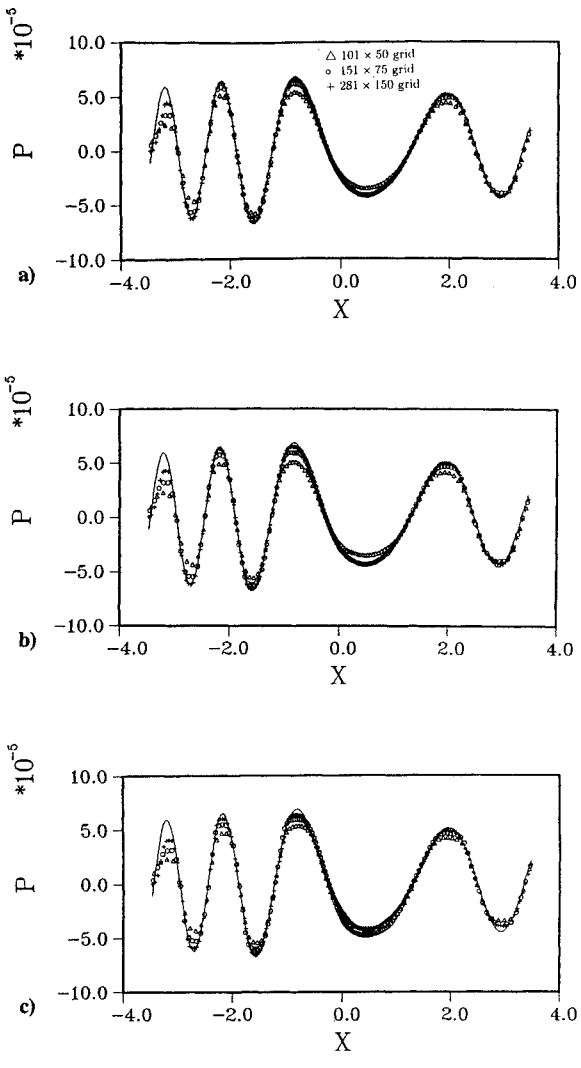

Fig. 8 Pressure plots at $y = 2.508$ obtained by schemes: a) MOC, b) OC, and c) LC.

show the errors and orders of accuracy of the LC scheme without and with the limiter, respectively. Since this scheme is only second-order accurate, it is not as good as the rest of schemes in computing smooth solutions.

The second initial condition is a combination of a sinusoidal and a discontinuous wave

$$u(t=0,x,y) = \begin{cases} 1+0.5\sin[2\pi(x+y)], & \text{for } 0 < x+y < 1 \\ 1.0 & \text{for } 1 < x+y < 1.4 \\ 1.5 & \text{for } 1.4 < x+y < 1.6 \\ 1.0 & \text{for } 1.6 < x+y < 2.0 \end{cases} \quad (15)$$

This test is to study the effects of discontinuities and limiter functions on each scheme. Figure 5a shows the u variation along the diagonal line computed by the MSL and LC schemes. The LC scheme produces some phase errors in this test. Figure 5b shows the same plot computed by the OC and MOC schemes. Again, the performance of the MOC scheme is slightly better than that of the OC scheme. To reduce the effect of the limiter function

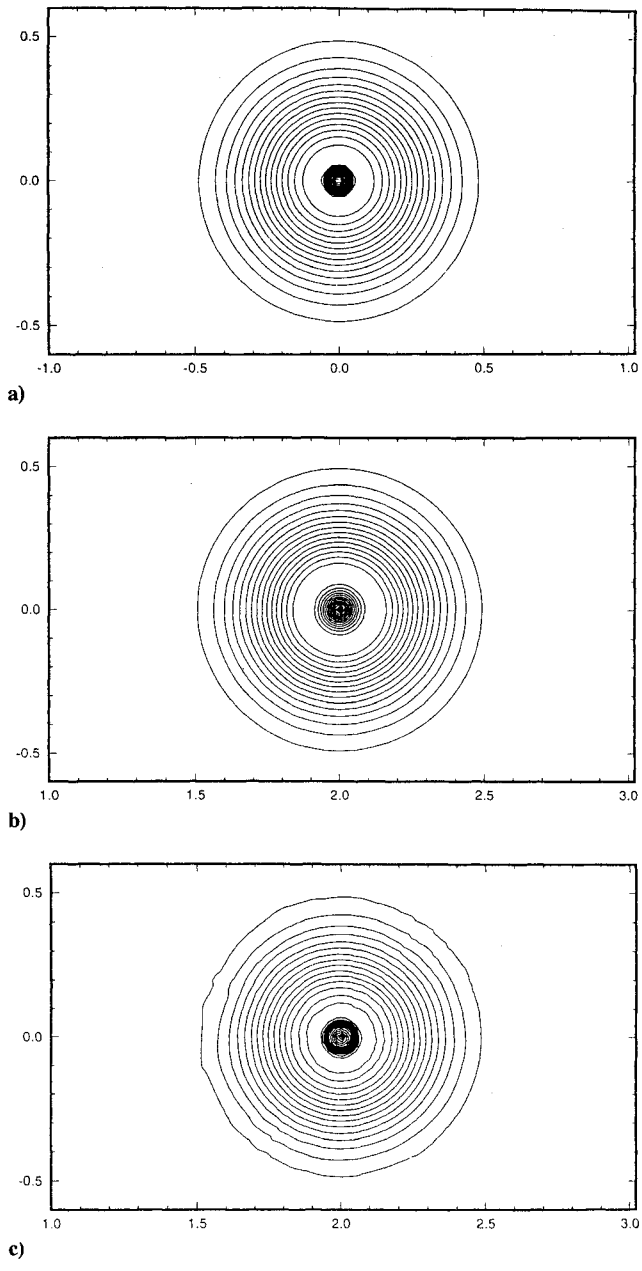

Fig. 9 Velocity contours for the traveling vortex test: a) initial data obtained by b) MOC scheme and c) MSL scheme.

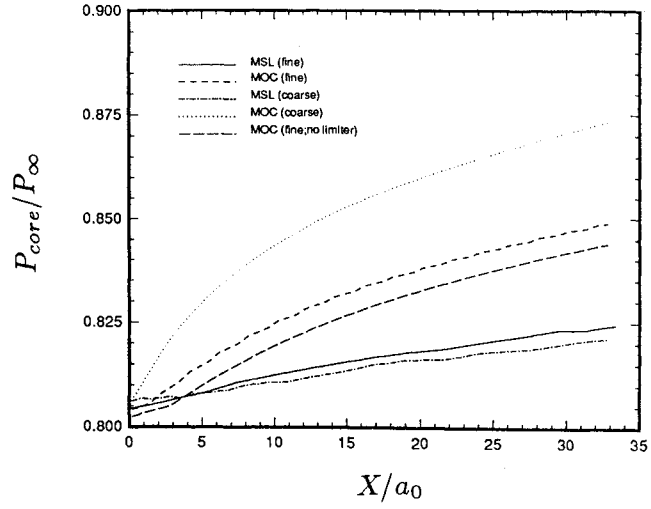

Fig. 10 Variation of the core pressure P_{core} as a function of the length of vortex travel.

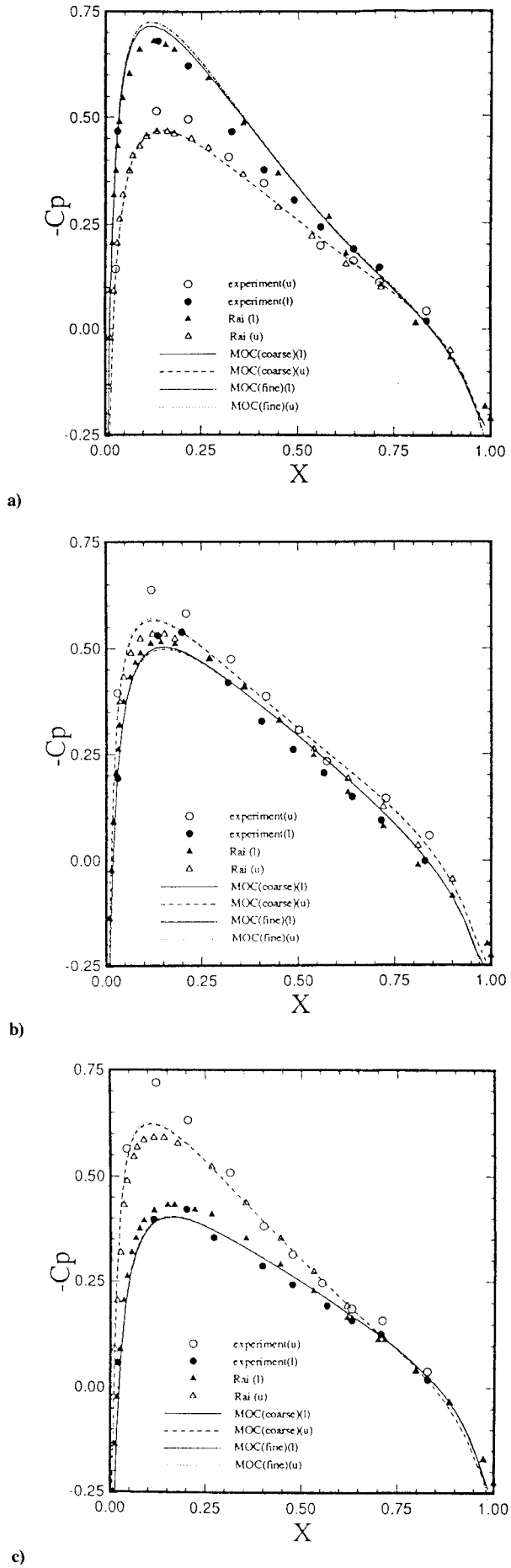

Fig. 11 Surface pressure distributions as a function of the position of the vortex: a) 0.289, b) 0.649, and c) 1.402.

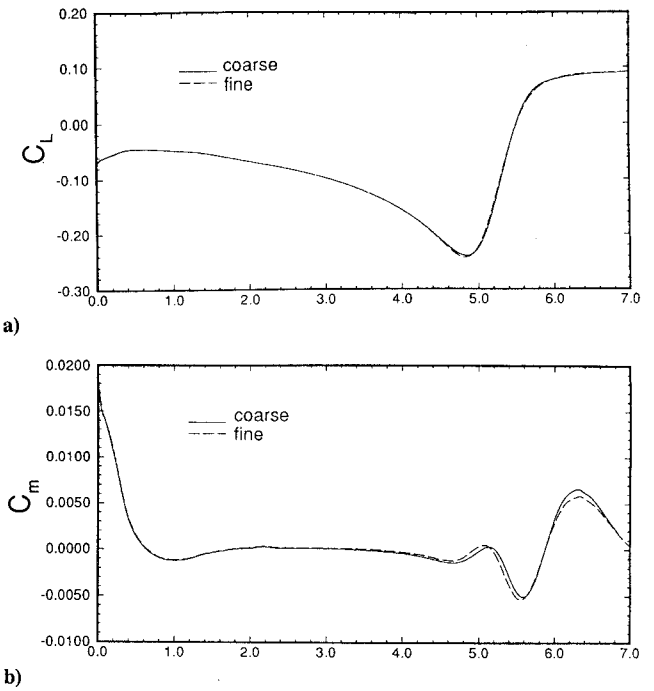

Fig. 12 Coefficients of a) lift and b) moment as a function of time.

in the extreme-point regions, we introduce the following TVB correction,[15] that is, $W^{R,(\mathrm{mod})}_{i-\frac{1}{2}}$ in Eq. (10) is replaced by

$$W^{R,(\mathrm{mod})}_{i-\frac{1}{2}} = \begin{cases} W^{R}_{i-\frac{1}{2}} & \text{if } \left|W_i - W^{R}_{i-\frac{1}{2}}\right| < M(\Delta_i x)^2 \\ W^{R,(\mathrm{mod})}_{i-\frac{1}{2}} & \text{otherwise} \end{cases} \tag{16}$$

where $\Delta_i x = x_{i+\frac{1}{2}} - x_{i-\frac{1}{2}}$ and M is a positive constant which generally depends on the second derivative of the computed solution. Similar treatment of $W^{L}_{i+\frac{1}{2}}$ is also performed. Figure 5b also shows the u variation obtained by the MOC scheme with different M values. Comparing the computed results obtained at $M = 5$ and 300, it is seen that the MOC scheme with $M = 5$ is good enough in this case.

C. Monopole Radiation in a Compressible Stream

We now consider a uniform stream past a monopole source in an infinite wall.[16] Figure 6 is a schematic of the problem. The volume flow rate emitted by the monopole source is $Q = 10^{-4} \times \sin(2\pi t)$ in a freestream with the Mach number of 0.2. The governing equations used are the Euler equations. The computational domain covers a finite region of $[-3.5, 3.5] \times [0, 3.5]$ and the monopole source is located at the origin. The dimensions of three grid systems used are shown in Table 9. Comparison of results is made at $t = 5$. The pressure at two y levels obtained by the MSL scheme are shown in Fig. 7. At $y = 1.26$, the scheme obtains accurate results on all of the grid systems. At $y = 2.508$, it only obtains accurate results on the finer grid. This is mainly due to the grid stretching in the y direction. The inaccuracy found in the upwind direction is also due to the grid stretching in the x direction. These results indicate that grid refinement is very important in acoustic computations. Figure 8 shows the pressure at $y = 2.508$ obtained by the MOC, OC, and LC schemes. It can be seen that the accuracy of the MOC scheme is slightly better than that of the OC scheme, whereas, around the extrema regions, the accuracy of the LC scheme cannot compete with that of the rest of the schemes. From the tests performed, the MSL and MOC appear to perform better than the other two schemes.

D. Traveling Vortex Test

In this section, a traveling vortex in a freestream[17] is tested using only the MSL and MOC schemes. The traveling vortex is described

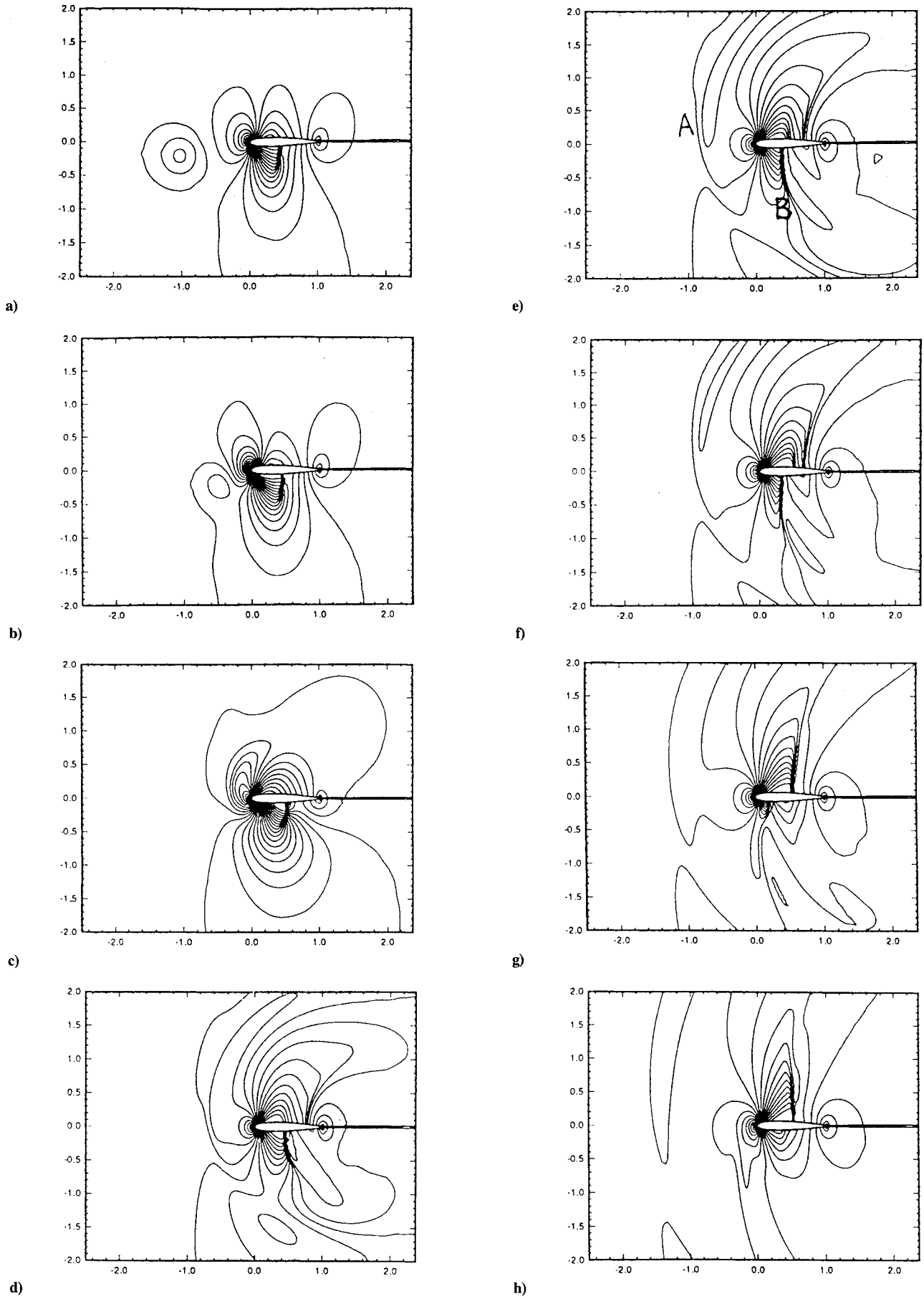

Fig. 13 Pressure contours as a function of time where A indicates the compressibility wave and B indicates the transonic wave.

initially by an analytical form of Sculley.[18] The angular velocity of the initial vortex is given as

$$\frac{v_\theta}{V_{\max}} = \begin{cases} r/a_0 & \text{if } r \le a_0 \\ \exp\left(-\dfrac{(r-a_0)^2}{\Omega}\right) & \text{if } r > a_0 \end{cases} \tag{17}$$

where $V_{\max} = 0.3$, $a_0 = 0.06$, and $\Omega = 0.065$. The pressure and density for the vortex are obtained from

$$\frac{dp}{dr} = \frac{\rho v_\theta^2}{r}$$

$$\frac{\gamma p}{(\gamma-1)\rho} + \frac{v_\theta^2}{2} = \frac{\gamma p_\infty}{(\gamma-1)\rho_\infty} \tag{18}$$

The pressure for such a vortex has a minimum at the center. The vortex is superimposed on a low-speed freestream with Mach number of 0.1. In a low-speed freestream, the change in pressure at the center is mainly due to the dissipation property of the numerical scheme used. The computational domain of $[-1, 4] \times [-1, 1]$ is uniformly divided by a fine grid, 333×133, or a coarse grid, 250×101. Figure 9a shows the velocity contours of the initial data. Figures 9b and 9c show the velocity contours obtained by the MOC and MSL schemes with the fine grid after 45 core radii of travel. Figure 10 shows the variation of the core pressure P_{core} as a function of the length of vortex travel. Clearly, the numerical dissipation of the MSL scheme is less than that of the MOC, but the solution using the MSL has small wiggles as shown in Fig. 9c. In Fig. 10, it is surprising that the MSL scheme seems to do better on the coarse grid. This may be due to the effect of the time accuracy. From this test and the oblique shock test we conclude that the MSL scheme needs to be improved in convergence before it is used to compute aeroacoustic solutions. Therefore, the MOC scheme is a good candidate for aeroacoustic computations.

E. Blade-Vortex Interaction

In this test, the velocity profile of a vortex is given by

$$v_\theta = \frac{\Gamma}{2\pi r}\left(\frac{r^2}{r^2 + a^2}\right) \tag{19}$$

where a (here $a = 0.164$) and r are the core radius and the distance from the center of the vortex, respectively; both are nondimensionalized by the chord length of the airfoil. Γ is the vortex strength, which is defined by the maximum circulation divided by the freestream velocity and the chord length. The sign of the vortex is defined negative for a clockwise flow direction.

First, we simulate a subsonic blade-vortex interaction problem with a freestream Mach number of 0.536. The vortex is superimposed at $(-5, -0.4)$, i.e., five chord lengths ahead the leading edge of a NACA 0012 airfoil and 0.4 chord lengths below the axis of symmetry. The vortex strength chosen is -0.2481. Two C-grid systems, 120×190 and 192×190, are used. Figure 11 shows the surface pressure distributions as a function of the position of the vortex. The results compare well with the experimental data[20] and other numerical results.[17] Figure 12 shows the lift and moment coefficients as a function of time. At the beginning, the lift is negative because the vortex induces a downwash near the leading edge of the airfoil. As the vortex passes the leading edge, the lift is increased to a positive value because the vortex induces an upwash on the airfoil. One can see that the results obtained by the fine and coarse grids are close to each other. Therefore, the coarse grid is used to compute a second blade-vortex interaction problem.

Here a transonic blade-vortex interaction problem with freestream Mach number of 0.76 is simulated. Recently, Lent et al.[10] found two sound waves, transonic and compressibility waves, in their experimental investigations. In our calculations, the vortex is superimposed at $(-5, -0.2)$. The vortex strength chosen is -0.3. Figure 13 shows the time history of pressure contours. In this figure, A indicates the compressibility wave, which propagates with velocity of $u - c$ upstream, and B indicates the transonic wave, which also propagates with velocity of $u - c$ upstream. The corresponding time-dependent pressure obtained at three points is shown in Fig. 14. The pressure decreases when the incoming vortex passes those points, and the pressure increases when each wave reaches those points.

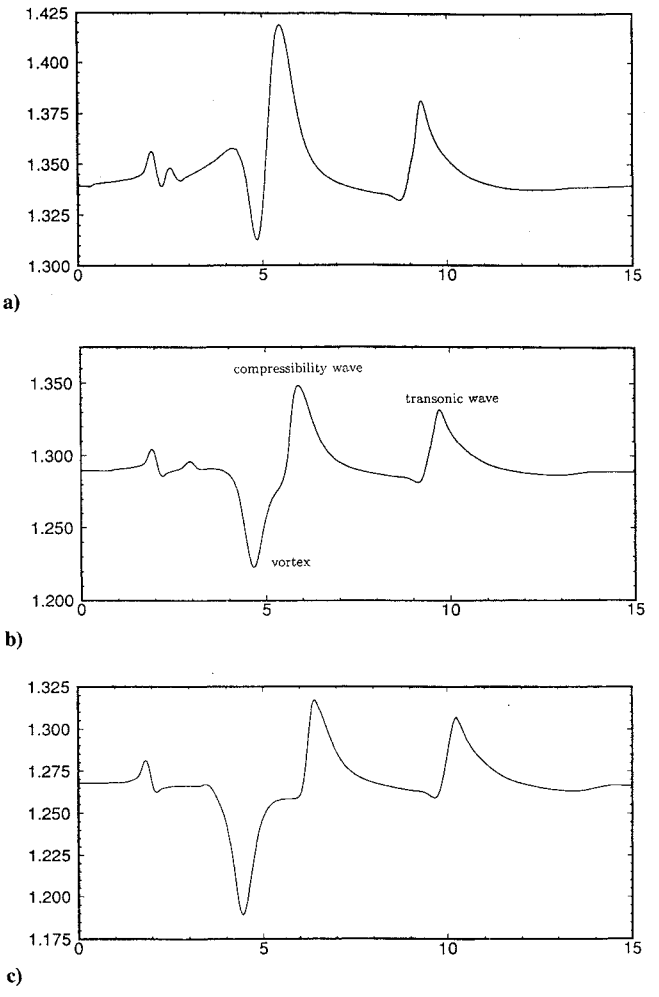

Fig. 14 Corresponding time-dependent pressure obtained at three points: a) (−0.2, −0.012), b) (−0.4, −0.016), and c) (−0.6, 0.019).

IV. Conclusions

A detailed investigation is made of the performance of several MUSCL schemes on several aerodynamic and aeroacoustic problems: oblique shock reflection, linear wave convection, monopole radiation, vortex preservation, and blade-vortex interaction. In the linear wave convection problem, the important effect of grid nonuniformity and the TVB limiter function is demonstrated. In the blade-vortex interaction problem, two sound waves, transonic and compressible waves, are simulated. Based on the order of accuracy, stability, effect of grid nonuniformity, and dissipation property of each scheme, we conclude that the MOC scheme is the most suitable scheme among those studied for aeroacoustic computations and that the MSL scheme needs to be improved to eliminate problems of convergence and small wiggles before it is used in computational aeroacoustics.

Acknowledgments

We thank the Institute of Aeronautics and Astronautics, National Cheng Kung University, for facility support. We also would like to thank reviewers and the associate editor for giving some valuable suggestions and for correcting our English.

References

[1] Van Leer, B., "Toward the Ultimate Conservative Difference Scheme V, A Second-Order Sequel to Godunov's Scheme," *Journal of Computational Physics*, Vol. 32, No. 1, 1979, pp. 101–136.

[2]Harten, A., "High Resolution Schemes for Hyperbolic Conservation Laws," *Journal of Computational Physics*, Vol. 49, No. 3, 1983, pp. 357–393.

[3]Osher, S., "Convergence of Generalized MUSCL Schemes," *SIAM Journal of Numerical Analysis*, Vol. 22, No. 5, 1984, pp. 947–961.

[4]Yee, H. C., "Construction of Explicit and Implicit Symmetric TVD Schemes and Their Applications," *Journal of Computational Physics*, Vol. 68, No. 1, 1987, pp. 151–179.

[5]Lin, S. Y., and Chin, Y. S., "Discontinuous Galerkin Finite Element Method for Euler and Navier-Stokes Equations," *AIAA Journal*, Vol. 31, No. 11, 1993, pp. 2016–2026.

[6]Lin, S. Y., Chin, Y. S., and Wang, Y. Y., "Numerical Investigations on Two-Dimensional Canard-Wing Aerodynamic Interference," *Journal of Aircraft* (to be published).

[7]Osher, S., and Chakravarthy, S. R., "High Resolution Schemes and the Entropy Condition," NASA-CR-172218, Sept. 1983.

[8]Sanders, R., and Li, C. P., "A Variation Nonexpansive Central Differencing Scheme for Nonlinear Hyperbolic Conservation Laws," *Proceedings of the Tenth Conference Computing Methods in Applied Science and Engineering* (Versailles, France), 1992, pp. 511–526.

[9]Li, C. P., and Shieh, T. H., "A Multigrid Nonoscillatory Method for Computing High Speed Flows," AIAA Paper 93-3319, July 1993.

[10]Lent, H. M., Meier, G. E. A., Muller, K. J., Obermeier, F., Schievelbusch, U., and Schurmann, "Mechanisms of Transonic Blade-Vortex Interaction Noise," *Journal of Aircraft*, Vol. 30, No. 1, 1993, pp. 88–93.

[11]Roe, P. L., "Approximate Riemann Solvers, Parameter Vectors and Difference Schemes," *Journal of Computational Physics*, Vol. 43, No. 2, 1981, pp. 357–372.

[12]Jameson, A., "Multigrid Algorithms for Compressible Flow Calculations," *Multigrid Method II*, edited by W. Hackbusch and V. Trottenberg, Lecture Notes in Mathematics, Vol. 1228, Springer-Verlag, Berlin, 1985, pp. 166–201.

[13]Lu, P. J., and Yeh, D. Y., "Transonic Flutter Suppression Using Active Acoustic Excitations," AIAA Paper 93-3285, July 1993.

[14]Chakravarthy, S. R., and Osher, S., "High Resolution Applications of the Osher Upwind Scheme for the Euler Equations," AIAA Paper 83-1943, July 1983.

[15]Lin, S. Y., Wu, T. M., and Chin, Y. S., "An Upwind Finite-Volume Scheme with a Triangular Mesh for Conservation Laws," *Journal of Computational Physics*, Vol. 107, No. 2, 1993, pp. 324–337.

[16]Yeh, D. Y., "Unsteady Aerodynamic and Aeroelastic Behaviors of Acoustically Excited Transonic Flow," Ph.D. Thesis, National Cheng Kung Univ., Tainan, Taiwan, ROC, 1992.

[17]Rai, M. M., "Navier-Stokes Simulations of Blade-Vortex Interaction Using High-Order Accurate Upwind Schemes," AIAA Paper 87-0543, Jan. 1987.

[18]Sculley, M. P., "Computation of Helicopter Rotor Wake Geometry and its Influence on Rotor Harmonic Loads," ASRL TR-178-1, Aeroelastic and Structure Research Lab., Massachusetts Inst. of Technology, March 1975.

[19]Meadows, K. R., Kumar, A., and Hussain, M. Y., "Computational Study on the Interaction Between a Vortex and a Shock Wave," *AIAA Journal*, Vol. 9, No. 2, 1991, pp. 174–179.

[20]Caradonna, F. X., Laub, G. H., and Tung, C., "An Experimental Investigation of the Parallel Blade-Vortex Interaction," *10th European Rotorcraft Forum*, The Hague, The Netherlands, Aug. 1984.